Provided for non-commercial research and education use.
Not for reproduction, distribution or commercial use.

This article appeared in a journal published by Elsevier. The attached copy is furnished to the author for internal non-commercial research and education use, including for instruction at the authors institution and sharing with colleagues.

Other uses, including reproduction and distribution, or selling or licensing copies, or posting to personal, institutional or third party websites are prohibited.

In most cases authors are permitted to post their version of the article (e.g. in Word or Tex form) to their personal website or institutional repository. Authors requiring further information regarding Elsevier's archiving and manuscript policies are encouraged to visit:

http://www.elsevier.com/copyright

Author's personal copy

Journal of Crystal Growth 314 (2011) 97–103

Contents lists available at ScienceDirect

Journal of Crystal Growth

journal homepage: www.elsevier.com/locate/jcrysgro

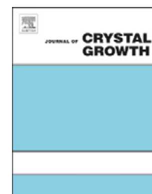

Epitaxial Mn-doped ZnO diluted magnetic semiconductor thin films grown by plasma-assisted molecular-beam epitaxy

Z. Yang [a,1], Z. Zuo [a], H.M. Zhou [a], W.P. Beyermann [b], J.L. Liu [a,*]

[a] *Quantum Structures Laboratory, Department of Electrical Engineering, University of California, Riverside, CA 92521, USA*
[b] *Department of Physics and Astronomy, University of California, Riverside, CA 92521, USA*

ARTICLE INFO

Article history:
Received 1 June 2010
Received in revised form
19 October 2010
Accepted 8 November 2010
Communicated by E. Calleja
Available online 18 November 2010

Keywords:
A3. Molecular beam epitaxy
B1. Oxide
B2. Semiconducting II–VI materials

ABSTRACT

A growth window for the Mn effusion cell temperature (T_{Mn}) is demonstrated for epitaxial Mn-doped ZnO (MnZnO) thin films grown on sapphire substrates using molecular-beam epitaxy. Within the growth window, the films are ferromagnetic with the largest saturated magnetization occurring at $T_{Mn}=700$ °C. The Curie temperature of these MnZnO diluted magnetic semiconductor thin films is above room-temperature. The ferromagnetism is weakly anisotropic. Well-resolved near-band-edge photoluminescence emissions dominate the spectra at both low- and room-temperatures. No evident spin polarization on the carriers was detected with the magneto-photoluminescence studies. Magnetoresistance and anomalous Hall effects of the MnZnO thin films were studied. The anomalous Hall coefficient shows a quadratic dependence on the resistivity.

© 2010 Elsevier B.V. All rights reserved.

1. Introduction

ZnO-based diluted magnetic semiconductor (DMS) materials have been widely studied in recent years [1,2], because of the theoretically predicted above-room-temperature Curie temperature [3,4]. The ferromagnetism has been observed in these systems using various material preparation methods [1,5–42]; however, epitaxial ZnO DMS thin films grown with precisely controllable techniques, such as molecular-beam epitaxy (MBE), have not been widely reported yet. The mechanism of magnetism in ZnO DMS is still controversial and needs further clarification. In this paper, we discuss the growth and characterizations of epitaxial ZnO DMS thin films on sapphire substrates using MBE, which is a continuation of our previous studies on hybrid MBE-implantation prepared ZnO DMS thin films [40–42].

2. Experiments

The MnZnO thin films were grown on *c*-plane sapphire substrates using plasma-assisted MBE. Before transferring to the MBE chamber, the sapphire substrates were chemically cleaned with hot (~150 °C) aqua regia (HNO_3:HCl = 1:3) solutions for 20 min, rinsed with de-ionized water, and dried with a nitrogen gun. Regular Knudsen effusion cells filled with elemental Zn (6 N) and Mn (5.5 N) were used as sources. An electron cyclotron resonance plasma tube supplied with O_2 (5 N) was used as the oxygen source [43]. The substrate temperature was kept at ~300 °C during the growth. Here, a relative low growth temperature was employed to facilitate the dopant incorporation [44,45]. The amount of Mn concentration in MnZnO was controlled by the Mn effusion cell temperature. A series of five MnZnO thin film samples were grown with Mn effusion cell temperature (T_{Mn}) varied from 620 to 780 °C with a step of 40 °C. While, the Zn cell temperature was kept at a constant of 390 °C. The detailed growth parameters of the five MnZnO samples were summarized in Table 1. During the following discussion of the structural, magnetic, optical, and transport properties, MnZnO thin film sample C was employed unless specified otherwise, which was grown with $T_{Mn}=700$ °C and shows the strongest magnetization.

X-ray photoelectron spectroscopy (XPS) was used to indentify elements and estimate the Mn concentration in the samples. X-ray diffraction (XRD) measurements were performed using a Bruker D8 Advance X-ray diffractometer. The resolution of XRD system is ~0.1°. Reflection high-energy electron diffraction (RHEED) measurements were performed *in situ* on the as-grown samples in the MBE system. Scanning electron microscopy (SEM) images were taken using a Philips XL 30 FEG SEM system. Atomic force microscopy (AFM) experiments were performed to investigate the surface roughness of the samples using a Veeco Dimension 5000 AFM system. Magnetic properties were measured with a Quantum Design MPMS-XL SQUID magnetometer. Photoluminescence (PL) measurements were carried out using a home-built

* Corresponding author. Tel.: +1 951 8277131; fax: +1 951 8272425.
E-mail address: jianlin@ee.ucr.edu (J.L. Liu).
[1] Present Address: School of Engineering and Applied Sciences, Harvard University, Cambridge, MA 02138, USA.

0022-0248/$ - see front matter © 2010 Elsevier B.V. All rights reserved.
doi:10.1016/j.jcrysgro.2010.11.059

Author's personal copy

Table 1
Growth parameters and Mn concentrations of $Mn_xZn_{1-x}O$ diluted magnetic semiconductor thin films.

Sample no.	T_{Growth} (°C)	T_{Zn} (°C)	T_{Mn} (°C)	Mn concentration	
				x (%)[a]	Description
A	~300	390	620	~1.8	$Mn_{0.02}Zn_{0.98}O$
B	~300	390	660	~4.3	$Mn_{0.04}Zn_{0.96}O$
C	~300	390	700	~7.7	$Mn_{0.08}Zn_{0.92}O$
D	~300	390	740	~9.3	$Mn_{0.09}Zn_{0.91}O$
E	~300	390	780	~12.6	$Mn_{0.13}Zn_{0.87}O$

[a] Refer to Fig. 1(c) for the error bar of Mn concentration x.

system with temperature control over a range of ~7–300 K in a Janis cryostat. A 325-nm wavelength Kimmon He–Cd laser was used as an excitation source and a photomultiplier tube was used to detect the PL signals. Field-dependent Hall effect and magnetoresistance (MR) measurements were performed using a Quantum Design PPMS system with magnetic fields up to 10 T.

3. Results and discussions

3.1. Structural properties

Fig. 1(a) shows the XPS spectra of MnZnO sample C with $T_{Mn}=700$ °C, with peaks relevant to Zn, O, and Mn elements observed. The C, Re, and Ta peaks in Fig. 1(a) arise from the contaminations of the sample mounting and sample holder in the XPS measurements. Fig. 1(b) shows the high-resolution XPS spectra of the same sample for Mn-3p and Zn-3p peaks, both of which are highlighted as red in Fig. 1(a). The Mn concentration x of each MnZnO sample was calculated using the following equation

$$x \approx \frac{(I_{Mn\text{-}3p}/RSF_{Mn\text{-}3p})}{(I_{Mn\text{-}3p}/RSF_{Mn\text{-}3p})+(I_{Zn\text{-}3p}/RSF_{Zn\text{-}3p})} \quad (1)$$

where $I_{Mn\text{-}3p}$ and $I_{Zn\text{-}3p}$ are integrated peak intensities of the Mn-3p and Zn-3p XPS peaks with a background in approximate Shirley shape [46,47] subtracted; while $RSF_{Mn\text{-}3p}$ and $RSF_{Zn\text{-}3p}$ are the XPS relative sensitivity factors of Mn-3p and Zn-3p peaks, with the values of 1.42 and 2.83, respectively, as shown in Fig. 1(b). The calculated Mn concentration of all the five samples is shown in Table 1. Fig. 1(c) shows the Arrhenius plot of the relation between the Mn concentrations (vertical-axis in percentage unit) and reciprocal of the Mn effusion cell temperatures (horizontal-axis). The error bars of Mn concentrations shown in Fig. 1(c) arise from the calculation uncertainties of the XPS peak integrated intensities. An Arrhenius fit (blue line in the figure) using relation

$$x \propto F_{Mn} \sim \exp\left(-\frac{E_a}{k_B T_{Mn}}\right) \quad (2)$$

was performed on the experimental data, employing the approximations that Mn concentration x is proportional to Mn flux (F_{Mn}) and F_{Mn} is in Arrhenius type of T_{Mn} as $\sim\exp(-E_a/k_BT_{Mn})$. The activation energy of Mn is approximately obtained as ~0.97 eV based on the fitting. This value is analyzed in the temperature range of 620–780 °C when Mn is used as a "dopant" source, which may significantly vary when it is used as a major compositional element source.

Fig. 2 shows the XRD pattern of the MnZnO epitaxial thin film sample C. Only MnZnO (0 0 0 2) and (0 0 0 4) peaks are observed at 34.8° and 73.0°, respectively, indicating that the film is well aligned along the c-direction. Besides the MnZnO peaks, a sapphire (0 0 0 6) peak is also observed at 42.0° from the substrate. Whether the sapphire substrate peak shows up [43,48,49] or not [40–42] depends on the thickness of the ZnO layer on top. The XRD peak position and full-width-at-half-maximum (FWHM) of the MnZnO (0 0 0 2) peaks from all the five samples are at 34.8° and ~0.30°, respectively. Neither Mn-related impurity phase peaks, nor evident Mn concentration dependence of the MnZnO (0 0 0 2) peak

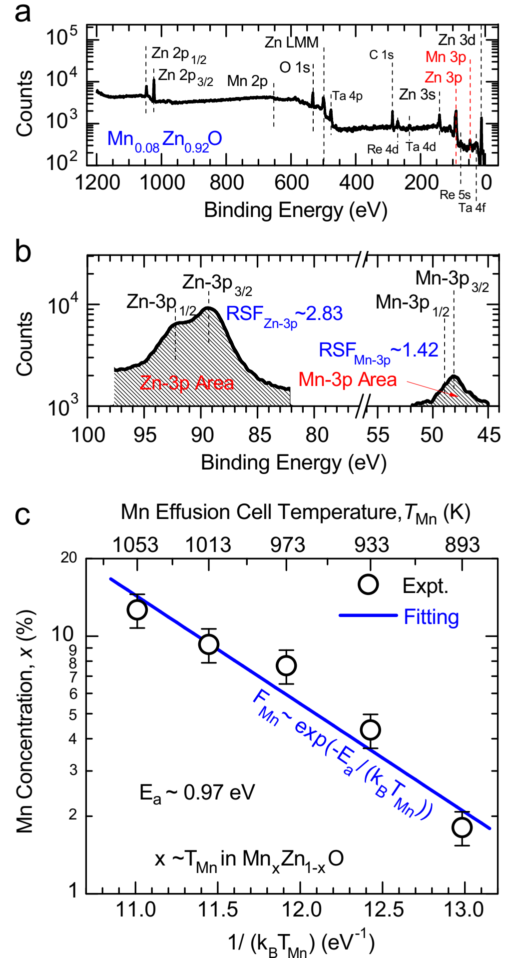

Fig. 1. (a) XPS spectra of MnZnO sample C. (b) High-resolution XPS spectra of Mn-3p and Zn-3p peaks for the same sample (c) Arrhenius plot of the relation between the Mn concentration x and Mn effusion cell temperature T_{Mn}.

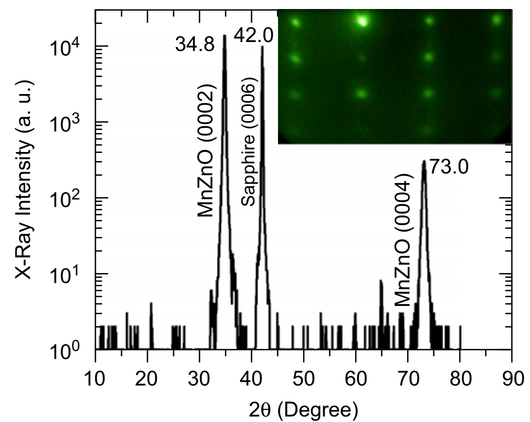

Fig. 2. XRD pattern of MnZnO sample C. The film is well aligned along c-direction. The inset shows the RHEED pattern of the film and the spotty pattern indicates a rough surface.

Author's personal copy

positions and FWHMs were observed within the detection and resolution limits of the XRD system. The latter is due to the relative small Mn concentrations (2–13%) in the samples. According to Ref. [50], the *c*-lattice constant of MnZnO only changes slightly from 0.521 to 0.523 nm, when Mn concentration in MnZnO increases from 0% to 10%. Hence, it is not too surprising that these tiny changes within 0.002 nm were not detected among these five MnZnO samples. A higher resolution XRD system may help clarify this issue in the future.

The inset in Fig. 2 shows the RHEED pattern of the MnZnO epitaxial thin film sample C. The spotty pattern indicates a rough surface of the MnZnO thin film. Fig. 3(a) shows an SEM image of the top surface of MnZnO sample C. The morphology of the film is strongly textured [51], which is consistent with the indication of a rough surface from the RHEED pattern, although the film is still well aligned along the *c*-direction as indicated by XRD. The scale bar of the SEM image is 1 μm. Fig. 3(b) shows the AFM image of the MnZnO sample C within a 1 μm × 1 μm area. The surface roughness of all the five MnZnO samples was characterized using AFM. The root-mean-square (RMS) surface roughness of MnZnO samples A–E are 19.7, 20.9, 23.3, 25.4, and 30.6 nm, respectively. The textured morphology and large surface roughness of the MnZnO samples are mainly due to the relatively low growth temperature (~300 °C) and Mn incorporation, since previous studies [49] show that the RMS surface roughness of undoped ZnO epitaxial thin films grown on sapphire substrates at high temperatures (>700 °C) can be optimized down to ~10 nm without buffer layers, and further down to <2 nm with low-temperature homo-buffers.

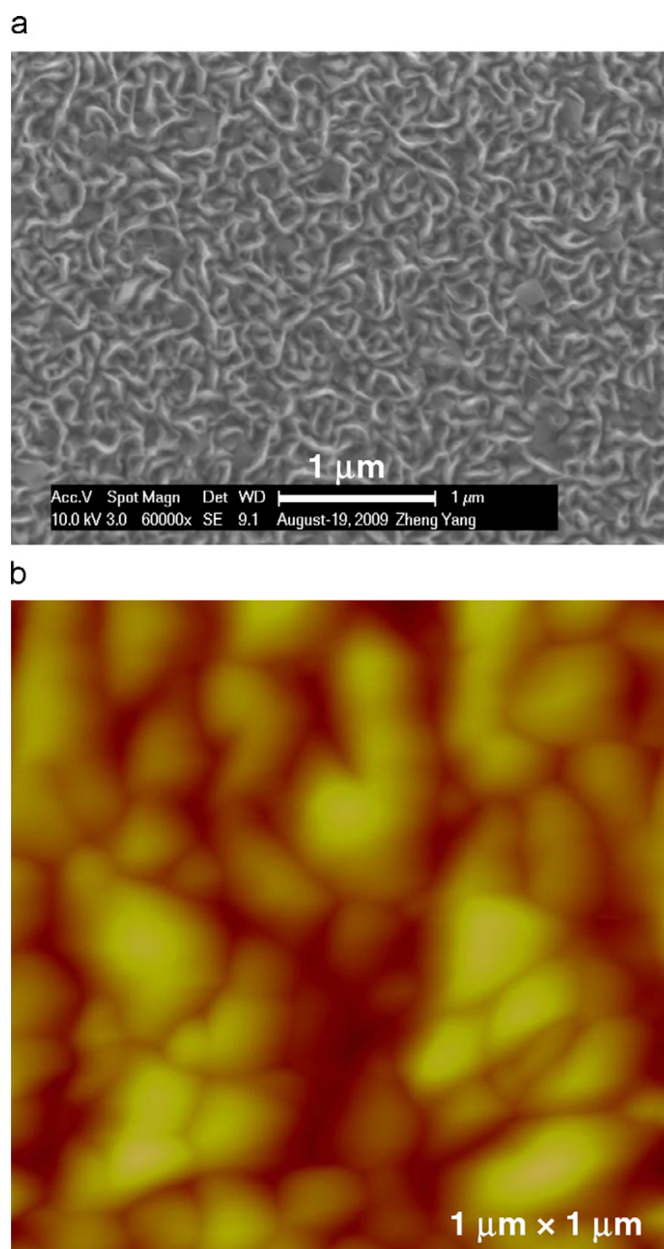

Fig. 3. (a) SEM image of the MnZnO sample C. The morphology of the film is strongly textured. (b) AFM image of the sample in 1 μm × 1 μm area.

3.2. Magnetic properties

Fig. 4(a)–(e) shows the magnetic field dependence of the 300-K magnetizations of MnZnO epitaxial thin film samples A–E. Samples A–E are prepared with the same growth parameters except for the different Mn effusion cell temperatures T_{Mn}, which ranges from 620 to 780 °C with a step of 40 °C (Table 1). Fig. 4(f) shows the plot of the saturated magnetization versus Mn effusion cell temperature for the five MnZnO samples, showing the dependence of the magnetic properties of the MnZnO samples on T_{Mn}. With increasing T_{Mn}, which corresponds to increased Mn incorporation, the saturated magnetization (M_s) of the MnZnO increases from ~7 emu cm^{-3} with T_{Mn}=620 °C to ~13 emu cm^{-3} with T_{Mn}=660 °C, and finally to ~22 emu cm^{-3} with T_{Mn}=700 °C. However, when T_{Mn} is further increased from 700 to 740 °C, M_s slightly decreases to ~19 emu cm^{-3}. At or beyond 780 °C, the magnetism is dominated by the diamagnetic behavior from the contribution of the sapphire substrate. This reduction in ferromagnetic character may suggest that the primary magnetic coupling mechanism between Mn ions in the MnZnO thin films changes gradually from a pure carrier-mediated one to a coexistence involving of both carrier mediation among Mn ions and direct exchange when a large amount of Mn is incorporated.

Fig. 5 shows the temperature dependence of the magnetization measured at 2.0 kOe for the MnZnO sample C. The magnetization only drops slightly with increase in temperature from 2 to 300 K, indicating a Curie temperature well above room-temperature. Fig. 6 shows the magnetic anisotropy of MnZnO sample C. The black and red curves show the magnetic field dependence of the magnetization with out-of-plane (magnetic field perpendicular to the film plan) and in-plane (magnetic field parallel to the film plane) geometries, respectively. The coercivity of the in-plane geometry is ~50 Oe, while the out-of-plane magnetization has a slightly larger coercivity. Generally clustering phases show isotropic magnetism; so the magnetic anisotropy is a sign of intrinsic ferromagnetism.

3.3. Optical properties

Fig. 7(a) shows the 9-K PL spectra of the MnZnO sample C. Several near-band-edge (NBE) peaks are observed in the PL spectra. The high-energy side shoulder peak at 3.363 eV is commonly assigned as the hydrogen donor-bound exciton (I_4 line) [52]. The dominating peaks at 3.243 and 3.306 eV are mainly proposed to be donor-acceptor-pair transitions [53,54], although other assignments have also been provided [55–57]. The inset shows the room-temperature PL spectra for the same sample. A dominating NBE peak at 3.25 eV and a weak and broad green band (GB) peak are observed. The GB emission is generally associated with oxygen vacancies in ZnO. The fact that well-resolved NBE peaks are observed and dominated in the PL spectra of the samples at both low- and room-temperature indicates a high quality of the epitaxial MnZnO DMS thin films. These were not observed in ZnO DMS thin

Author's personal copy

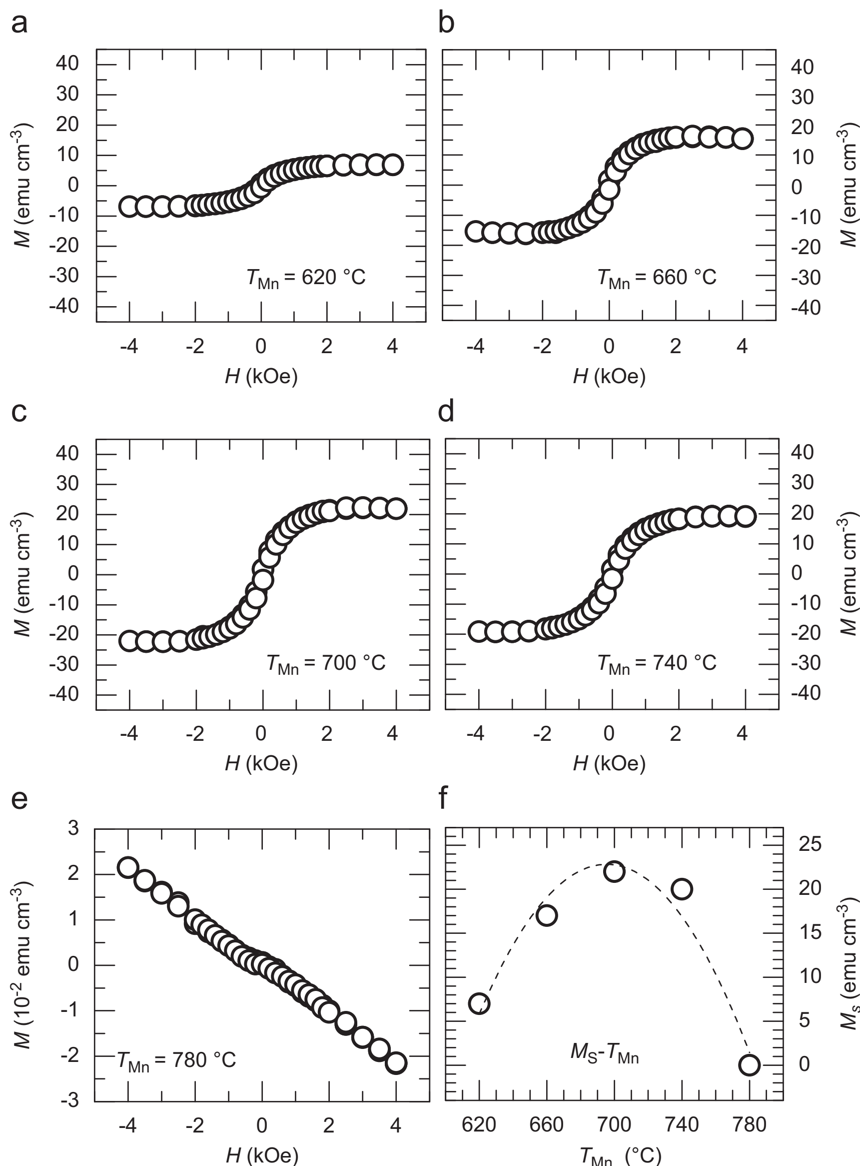

Fig. 4. (a)–(e) Magnetic field dependence of the magnetization measured at 300 K for MnZnO epitaxial thin films on sapphire (samples A–E) with the same growth parameters except for the Mn effusion cell temperature ranging from 620 °C to 780 °C in steps of 40 °C. (f) Plot of the saturated moment versus Mn effusion cell temperatures for MnZnO samples A–E.

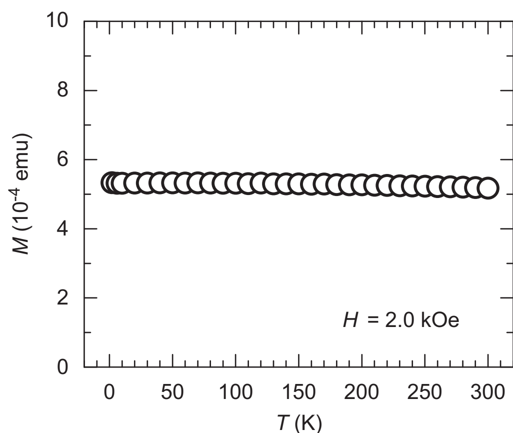

Fig. 5. Temperature dependence of the magnetization measured at 2.0 kOe for the MnZnO sample C. The magnetization only drops slightly with temperature increasing from 2 to 300 K, indicating a Curie temperature far-above room-temperature.

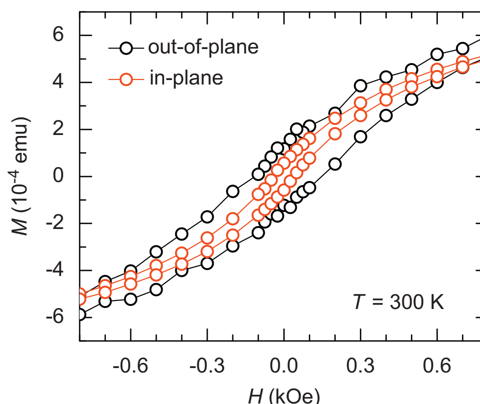

Fig. 6. Magnetic anisotropy of MnZnO sample C. The black and red curves show the magnetic field dependence of the magnetization with out-of-plane and in-plane geometries, respectively. The out-of-plane curve shows a slightly larger coercivity. (For interpretation of the references to color in this figure legend, the reader is referred to the web version of this article.)

Author's personal copy

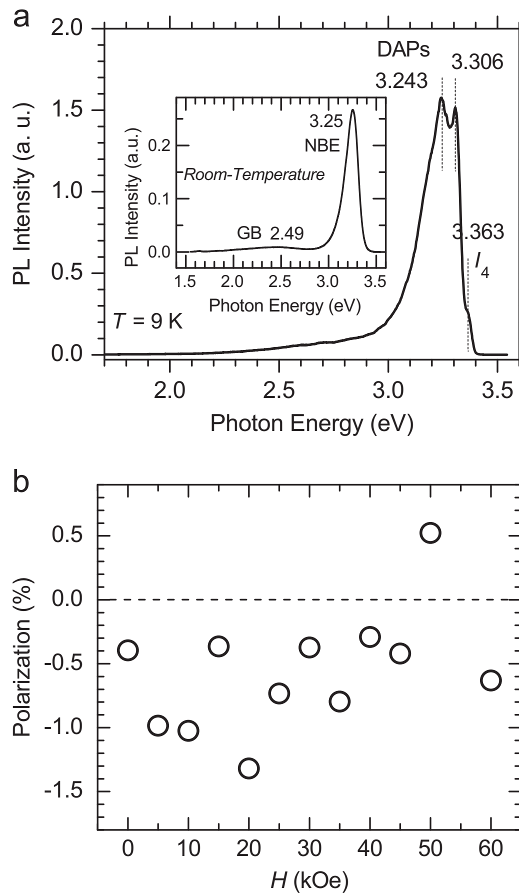

Fig. 7. (a) Photoluminescence spectra of MnZnO sample C measured at 9 K. The inset shows the room-temperature PL spectra of the same sample. (b) Spin polarization statistics, determined from the magneto-PL of the same sample at ~7 K for different magnetic fields up to 6 T.

films with implanted magnetic ions [40–42], where the PL spectra are dominated by deep-level emissions.

Fig. 7(b) shows the spin polarization statistical graph at different magnetic fields (up to 6 T) derived from magneto-PL studies at ~7 K. The spin polarization is defined as the difference between the right- and left-circular-polarized PL intensity divided by the sum of the two. No evident carrier spin polarization is observed. Recently, Chen et al. [58] pointed out that two dominating factors may limit the efficiency of optical spin detection in ZnO-based materials, which are the weak spin-orbit interactions and the fast carrier/exciton spin relaxations in ZnO. According to their analyses [58], the weak spin-orbit coupling (-3.5–16 meV [58–64]) leads to the cancellation of the circular polarization from the optical transitions between the conduction band and valence band states in ZnO and the spin relaxation is very fast (45–80 ps at 2 K [58]) especially when the ZnO is of high impurity density [58]. Our recent studies [65] based on time-resolved optical orientation measurements also show that the spin coherence time in ZnO is significantly decreased when the density of "impurity" states increases. These may be the possible reasons for no observation of spin polarization in our magneto-PL studies. However, some successful magneto-optical studies [60,61,65–71] have also been reported, despite of the two claimed "dominating factors" [58]. For example, long electron spin coherence times (up to 20 ns at 30 K [66]) were observed in "relatively clean" undoped ZnO samples using time-resolved Faraday/Kerr rotation spectroscopy at low-temperatures [65–68], and even at elevated temperatures (188 ps at 280 K [66]); a not short hole spin coherence time (350 ps at 1.7 K) in ZnO [61] and a not small polarization (11% at 20 K [60]) together with a not short decay time (275 ps at 20 K [60]) of donor-bound exciton were observed in ZnO using time-resolved magneto-PL studies; evident free [69] and bound [70] exciton splittings were observed in ZnO-based DMS materials using magnetic-optical techniques and well explained [71]. So these distinct results (unsuccessful vs. successful optical spin detections of ZnO) suggest that the "intrinsic background impurity/defect states" of ZnO, which differs significantly from samples to samples prepared with different methods, more or less determine the possibility of optical spin detections in ZnO also. The DAP peaks dominate in the magneto-PL spectra of all our five MnZnO samples, which is frequently seen in doped ZnO samples, while only a weak hydrogen donor-bound exciton peak (I_4) shows on the right shoulder of the main DAP peak. No magnetic field dependence of this shoulder exciton-related peak was evidently observed. Finally, it is worthwhile to point out here that ZnO DMS samples with exciton (either bound or free) dominant PL spectra may provide a more reliable way on exciton splitting analyses in magneto-PL, because it is more precise to define the peak position of a dominant peak than a shoulder peak.

3.4. Transport properties

In magnetic materials, the Hall resistance is contributed by both the ordinary and anomalous Hall effects (AHEs) and is expressed as

$$R_{Hall} = \frac{R_0}{d}(\mu_0 H) + \frac{R_s}{d}(\mu_0 M) \quad (3)$$

where R_0 and R_S are the ordinary and anomalous Hall coefficients, respectively, d is the thickness of the film, H and M are the magnetic field and magnetization perpendicular to the film plane, respectively, and μ_0 is the free space permeability. The anomalous Hall coefficient R_S can be extracted by extrapolation of the linear fit to the high field Hall resistance to zero field, as discussed in detail previously [42]. Fig. 8(a) shows temperature dependence of the anomalous Hall coefficient of the MnZnO thin film with the inset showing the temperature dependence of the resistivity ρ_x. By examining the relation between R_S and ρ_x, the (scattering) mechanisms for charge carriers in the MnZnO thin film can be determined [42]. R_S has both linear and quadratic dependence on ρ_x, and it can be expressed as

$$R_S = a_{sk}\rho_x + b_{sj}\rho_x^2 \quad (4)$$

The linear term is interpreted as the skew scattering and the quadratic term is associated with side-jump scattering or intrinsic mechanisms. Fig. 8(b) shows a plot of R_S/ρ_x versus ρ_x. The square symbols with error bar are the experimental data and the dashed line is a linear fit. The linear fit represents the dominance of the quadratic dependence. From the fitting, the parameters are $a_{sk} = (-3.3 \pm 0.7) \times 10^{-7}\ \mathrm{Gs}^{-1}$ and $b_{sj} = (2.0 \pm 0.4) \times 10^{-6}\ \mathrm{Gs}^{-1}\,\Omega^{-1}\,\mathrm{cm}^{-1}$, respectively. Based on parameter a_{sk}, the skew scattering angle is estimated to be -0.4 to -0.3 mRad. Early studies tended to assume the existence of the quadratic term is a possible indication of intrinsic carrier-mediation ferromagnetism [72,73]. However, recent AHE studies [74] classify both screw-scattering and side jump terms as extrinsic mechanisms to AHE, while a contribution, which only depends on bands structure but is independent of scattering process, is defined as intrinsic mechanism. In side-jump and intrinsic mechanisms the anomalous Hall coefficients are quadrically dependent on resistivity, while linear dependence dominates in the skew-scattering mechanism. The anomalous Hall coefficient dependence on the resistivity is in its prematured stage and controversial. Recent studies [75] show that the AHE can also be observed in paramagnetic two-dimensional electron gas systems, which makes the mechanism of AHE more debatable. Here, although it is difficult to conclude the intrinsic mechanism from the quadratic dependence shown in Fig. 8(b), the fitting of the quadratic dependence

Author's personal copy

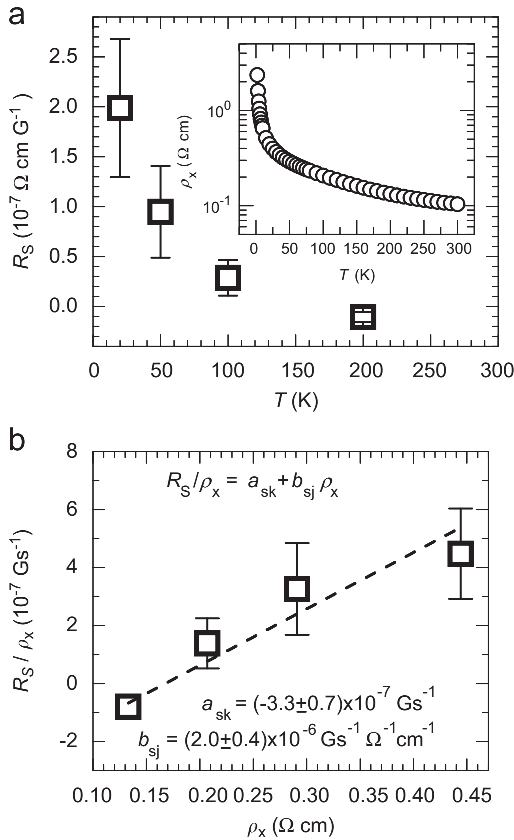

Fig. 8. (a) Temperature dependence of the anomalous Hall coefficient R_S for MnZnO sample C. The inset shows the temperature dependence of the resistivity for the same sample. (b) The plot of R_S/ρ_x versus ρ_x. The dashed line is a linear fit, indicating R_S has both linear and quadratic dependence on ρ_x. The two fitting parameters were listed in the graph.

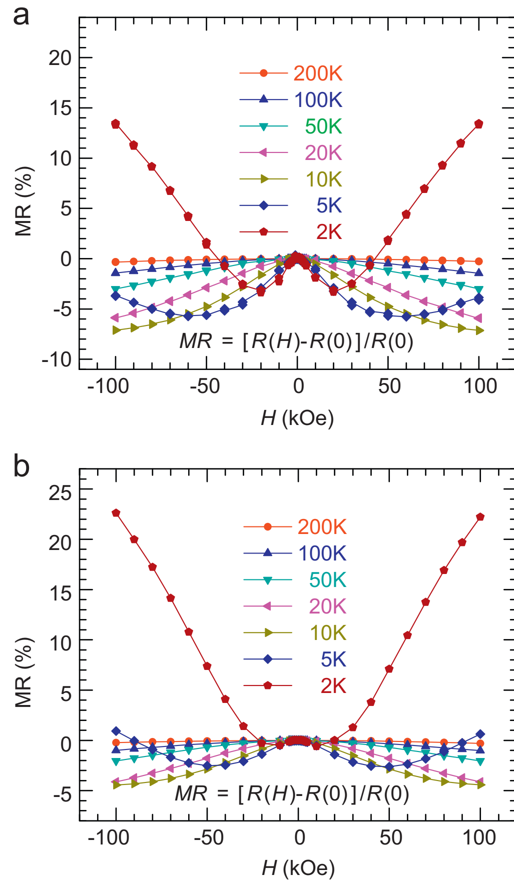

Fig. 9. Magnetoresistance of MnZnO sample C measured from 2 to 200 K with (a) out-of-plane MR and (b) in-plane MR geometries.

and fitting parameters discussed therein can be useful for future studies.

Fig. 9(a) and (b) shows the MR for the MnZnO thin film at 2, 5, 10, 20, 50, 100, and 200 K with magnetic fields up to 10 T in the out-of-plane and in-plane geometries. MR is defined as $MR=[R(H)-R(0)]/R(0)$. The out-of-plane and in-plane MR curves show similar shape, indicating the same scattering mechanism, but slightly different magnitudes are observed due to the anisotropic magnetism in the MnZnO thin film. At 2 K, MR is dominated by a positive contribution, and as the temperature is increased the competition from a negative component increases and is very apparent at 5 K. Above 5 K, the MR is clearly negative. The positive MR is attributed to a giant spin-splitting of band states caused by a sp–d exchange interaction in DMSs while the negative MR could be from either weak localization or bound magnetic polarons [42]. These discussions are consistent with the MR studied in MnZnO:Al (with electron carrier concentrations on the order of $\sim 10^{20}$ cm^{-3}) [76], in which the positive and negative MR of MnZnO were also attributed to giant spin-splitting of the conduction band and formation of bound magnetic polarons.

The main point of this paper is the experimental demonstration of a growth window for MBE-grown MnZnO epitaxial thin films, within which the MnZnO samples show “ferromagnetism”. Although only the magnetization measurements strongly confirm the ferromagnetism (which is the reason of putting a quotation mark there), while neither transport nor optical measurements show additionally strong support to the intrinsic mechanism of the ferromagnetism, the experimental results discussed in the paper pave the way to the investigation of Mn concentration dependence of the magnetization in MnZnO. Tremendous efforts are still required to further clarify the real origins and mechanisms of the ferromagnetism in ZnO-based DMS materials. The studies of ZnO-based DMS are still controversial now, and seem to be more controversial instead of reaching agreements after more experimental results are reported. This is due to the hosting material—ZnO itself. We believe that a more reliable platform for ZnO DMS studies will be forming, if the properties of hosting ZnO materials (before magnetic doping), such as background donor impurity species and density, mobility, and crystallinity, do not show significant difference among different research groups in ZnO DMS community. The current status is still far away from that, for example, the background electron concentration and mobility of undoped ZnO show several orders of magnitude of difference from groups to groups. Starting from a quite distinct platform, it is evidently not surprising that the ZnO DMS show different properties after magnetically doped. Further comparisons among these results are more likely to lead to controversies rather than clarifications. This is somehow true for GaN-based DMS [1] and other oxide-based DMS [2] materials also, unlike the classic semiconductors such as GaAs, for which many different groups and companies can obtain same crystallinity samples with almost identical intrinsic carrier concentration and mobility.

4. Summary

In summary, MnZnO DMS thin films were grown on sapphire substrates using MBE. The MnZnO DMS thin films are well aligned along the *c*-direction according to XRD, although their surfaces are rough and textured as indicated by RHEED and SEM. No impurity phase segregation was observed in the XRD patterns within the

Author's personal copy

system detection limit. It has been demonstrated that an effusion cell temperature of Mn between 620 and 740 °C is the effective growth window for ferromagnetic films with the largest saturated magnetization shown at a cell temperature of 700 °C. The ferromagnetism in the MnZnO DMS thin films shows an above-room-temperature Curie temperature and a weak anisotropy. In the PL spectra, well-resolved NBE PL peaks dominate at both low- and room-temperatures, indicating high-quality MBE-grown MnZnO DMS thin films. No evident spin polarization of the carriers was detected with the magneto-photoluminescence studies. Positive and negative magnetoresistances were observed below and above 5 K, respectively. Anomalous Hall effects were observed in the MnZnO DMS thin films, with a quadratic dependence of the anomalous Hall coefficient on the resistivity observed.

Acknowledgement

This work was supported by ONR/DMEA through the Center of Nanomaterials and Nanodevice (CNN) under the award no. H94003-08-2-0803. The authors would like to thank Prof. Hao Zeng in University at Buffalo (SUNY) for the magneto-PL measurements.

References

[1] C. Liu, F. Yun, H. Morkoç, J. Mater. Sci: Mater. Electron. 16 (2005) 555.
[2] S.J. Pearton, W.H. Heo, M. Ivill, D.P. Norton, T. Steiner, Semicond. Sci. Technol. 19 (2004) R59.
[3] T. Dietl, H. Ohno, F. Matsukura, J. Cibert, D. Ferrand, Science 287 (2000) 1019.
[4] K. Sato, H. Katayama-Yoshida, Semicond. Sci. Technol. 17 (2002) 367.
[5] Z. Jin, T. Fukumura, M. Kawasaki, K. Ando, H. Saito, T. Sekiguchi, Y.Z. Yoo, M. Murakami, Y. Matsumoto, T. Hasegawa, H. Koinuma, Appl. Phys. Lett. 78 (2001) 3824.
[6] K. Ueda, H. Tabata, T. Kawai, Appl. Phys. Lett. 79 (2001) 988.
[7] W. Jung, S.-J. An, G.-C. Yi, C.U. Jung, S.-I. Lee, S. Cho, Appl. Phys. Lett. 80 (2002) 4561.
[8] P. Sharma, A. Gupta, K.V. Rao, Frank J. Owens, R. Sharma, R. Ahuja, J.M. Osorio Guillen, B. Johansson, G.A. Gehring, Nat. Mater. 2 (2003) 673.
[9] D.P. Norton, S.J. Pearton, A.F. Hebard, N. Theodoropoulou, L.A. Boatner, R.G. Wilson, Appl. Phys. Lett. 82 (2003) 239.
[10] S. Ramachandran, A. Tiwari, J. Narayan, Appl. Phys. Lett. 84 (2004) 5255.
[11] J.M. Baik, J.-L. Lee, Adv. Mater. 17 (2005) 2745.
[12] O.D. Jayakumar, I.K. Gopalakrishnan, S.K. Kulshreshtha, Adv. Mater. 18 (2006) 1857.
[13] X. Wang, J. Xu, B. Zhang, H. Yu, J. Wang, X. Zhang, J. Yu, Q. Li, Adv. Mater. 18 (2006) 2476.
[14] M. Bouloudenine, N. Viart, S. Colis, J. Kortus, a. Dinia, Appl. Phys. Lett. 87 (2005) 052501.
[15] D.A. Schwartz, D.R. Gamelin, Adv. Mater. 16 (2004) 2115.
[16] N. Khare, M.J. Kappers, M. Wei, M.G. Blamire, J.L. MacManus-Driscoll, Adv. Mater. 18 (2006) 1449.
[17] M.H.F. Sluiter, Y. Kawazoe, P. Sharma, A. Inoue, A.R. Raju, C. Rout, U.V. Waghmare, Phys. Rev. Lett. 94 (2005) 187204.
[18] K.R. Kittilstved, D.A. Schwartz, A.C. Tuan, S.M. Heald, S.A. Chambers, D.R. Gamelin, Phys. Rev. Lett. 97 (2006) 037203.
[19] J. Alaria, H. Bieber, S. Colis, G. Schmerber, A. Dinia, Appl. Phys. Lett. 88 (2006) 112503.
[20] X.C. Liu, E.W. Shi, Z.Z. Chen, H.W. Zhang, B. Xiao, L.X. Song, Appl. Phys. Lett. 88 (2006) 252503.
[21] T. Zhang, L.X. Song, Z.Z. Chen, E.W. Shi, L.X. Chao, H.W. Zhang, Appl. Phys. Lett. 89 (2006) 172502.
[22] M. Venkatesan, P. Stamenov, L.S. Dorneles, R.D. Gunning, B. Bernoux, J.M.D. Coey, Appl. Phys. Lett. 90 (2007) 242508.
[23] K.R. Kittilstved, N.S. Norberg, D.R. Gamelin, Phys. Rev. Lett. 94 (2005) 147209.
[24] Z.B. Gu, M.H. Lu, J. Wang, D. Wu, S.T. Zhang, X.K. Meng, Y.Y. Zhu, S.N. Zhu, Y.F. Chen, X.Q. Pan, Appl. Phys. Lett. 88 (2006) 082111.
[25] H.Y. Xu, Y.C. Liu, C.S. Xu, Y.X. Liu, C.L. Shao, R. Mu, Appl. Phys. Lett. 88 (2006) 242502.
[26] W. Yan, Z. Sun, Q. Liu, Z. Li, T. Shi, F. Wang, Z. Qi, G. Zhang, S. Wei, H. Zhang, Z. Chen, Appl. Phys. Lett. 90 (2007) 242509.
[27] Q. Wan, Appl. Phys. Lett. 89 (2006) 082515.
[28] M. Ivill, S.J. Pearton, Y.W. Heo, J. Kelly, A.F. Hebard, D.P. Norton, J. Appl. Phys. 101 (2007) 123909.
[29] K. Lord, T.M. Williams, D. Hunter, K. Zhang, J. Dadson, A.K. Pradhan, Appl. Phys. Lett. 88 (2006) 262105.
[30] S. Lee, D.Y. Kim, Y. Shon, C.S. Yoon, Appl. Phys. Lett. 89 (2006) 022120.
[31] Y.Z. Peng, T. Liew, T.C. Chong, C.W. An, W.D. Song, Appl. Phys. Lett. 88 (2006) 192110.
[32] Q. Xu, L. Hartmann, H. Schmidt, H. Hochmuth, M. Lorenz, R. Schmidt-Grund, C. Sturm, D. Spemann, M. Grundmann, Phys. Rev. B 73 (2006) 205342.
[33] Q. Xu, L. Hartmann, H. Schmidt, H. Hochmuth, M. Lorenz, R. Schmidt-Grund, C. Sturm, D. Spemann, M. Grundmann, Y. Liu, J. Appl. Phys. 101 (2007) 063918.
[34] W. Shim, K. Lee, W. Lee, K.A. Jeon, S.Y. Lee, M.H. Jung, J. Appl. Phys. 101 (2007) 123908.
[35] H. Pan, J.B. Yi, L. Shen, R.Q. Wu, J.H. Yang, J.Y. Lin, Y.P. Feng, J. Ding, L.H. Van, J.H. Yin, Phys. Rev. Lett. 99 (2007) 127201.
[36] J.M.D. Coey, M. Venkatesan, C.B. Fitzgerald, Nat. Mater. 4 (2005) 173.
[37] P. Sati, R. Hayn, R. Kuzian, S. Régnier, S. Schäfer, A. Stepanov, C. Morhain, C. Deparis, M. Laügt, M. Goiran, Z. Golacki, Phys. Rev. Lett. 96 (2006) 017203.
[38] C. Song, K.W. Geng, F. Zeng, X.B. Wang, Y.X. Sheng, F. Pan, Y.N. Xie, T. Liu, T.T. Zhou, Z. Fan, Phys. Rev. B 73 (2006) 024405.
[39] A. Zukova, A. Teiserskis, S. Van Dijken, Y.K. Gun'Ko, V. Kazlauskiene, Appl. Phys. Lett. 89 (2006) 232503.
[40] Z. Yang, J.L. Liu, M. Biasini, W.P. Beyermann, Appl. Phys. Lett. 92 (2008) 042111.
[41] Z. Yang, M. Biasini, W.P. Beyermann, M.B. Katz, O.K. Ezekoye, X.Q. Pan, Y. Pu, J. Shi, Z. Zuo, J.L. Liu, J. Appl. Phys. 104 (2008) 113712.
[42] Z. Yang, W.P. Beyermann, M.B. Katz, O.K. Ezekoye, Z. Zuo, Y. Pu, J. Shi, X.Q. Pan, J.L. Liu, J. Appl. Phys. 105 (2009) 053708.
[43] Z. Yang, J.–H. Lim, S. Chu, Z. Zuo, J.L. Liu, Appl. Surf. Sci. 255 (2008) 3375.
[44] L. Li, Z. Yang, J.Y. Kong, J.L. Liu, Appl. Phys. Lett. 95 (2009) 232117.
[45] Z. Yang, L. Li, Z. Zuo, J.L. Liu, J. Cryst. Growth 312 (2009) 68.
[46] Z. Yang, C. Ko, S. Ramanathan, J. Appl. Phys. 108 (2010) 073708.
[47] Z. Yang, C. Ko, V. Balakrishnan, G. Gopalakrishnan, and S. Ramanathan, Phys. Rev. B 82 (2010) 205101.
[48] Z. Yang, S. Chu, W.V. Chen, L. Li, J. Kong, J. Ren, P.K.L. Yu, J.L. Liu, Appl. Phys. Express 3 (2010) 032101.
[49] Z. Yang, H.M. Zhou, W.V. Chen, L. Li, J.Z. Zhao, P.K.L. Yu, J.L. Liu, J. Appl. Phys. 108 (2010) 066101.
[50] T. Fukumura, Z. Jin, A. Ohtomo, H. Koinuma, M. Kawasaki, Appl. Phys. Lett. 75 (1999) 3366.
[51] E.F. Schubert, Light-Emitting Diodes, Cambridge, 2006.
[52] B.K. Meyer, H. Alves, D.M. Hofmann, W. Kriegseis, D. Forster, F. Bertram, J. Christen, A. Hoffmann, M. Straßburg, M. Dworzak, U. Haboeck, A.V. Rodina, Phys. Status Solidi B 241 (2004) 231.
[53] Z. Yang, D.C. Look, J.L. Liu, Appl. Phys. Lett. 94 (2009) 072101.
[54] Z. Yang, J.L. Liu, J. Vac. Sci. Tech. B 28 (2010) C3D6.
[55] M. Schirra, R. Schneider, A. Reiser, G.M. Prinz, M. Feneberg, J. Biskupek, U. Kaiser, C.E. Krill, K. Thonke, R. Sauer, Phys. Rev. B 77 (2008) 125215.
[56] K. Thonke, M. Schirra, R. Schneider, A. Reiser, G.M. Prinz, M. Feneberg, R. Sauer, J. Biskupek, U. Kaiser, Phys. Status Solidi B 247 (2010) 1464.
[57] S.S. Kurbanov, T.W. Kang, J. Lumin. 130 (2010) 767.
[58] W.M. Chen, I.A. Buyanova, a. Murayama, T. Furuta, Y. Oka, D.P. Norton, S.J. Pearton, A. Osinsky, J.W. Dong, Appl. Phys. Lett. 92 (2008) 092103.
[59] N.J. Harmon, W.O. Putikka, R. Joynt, Phys. Rev. B 79 (2009) 115204.
[60] D. Lagarde, L. Lombez, A. Balocchi, P. Renucci, H. Carrère, T. Amand, X. Marie, Z.X. Mei, X.L. Du, Q.K. Xue, Phys. Status Solidi C 4 (2007) 472.
[61] D. Lagarde, A. Balocchi, P. Renucci, H. Carrère, F. Zhao, T. Amand, X. Marie, Z.X. Mei, X.L. Du, Q.K. Xue, Phys. Rev. B 78 (2008) 033203.
[62] D.C. Reynolds, D.C. Look, B. Jogai, C.W. Litton, G. Cantwell, W.C. Harsch, Phys. Rev. B 60 (1999) 2340.
[63] B. Gil, Phys. Rev. B 64 (2001) 201310(R).
[64] W.R.L. Lambrecht, A.V. Rodina, S. Limpijumnong, B. Segall, B.K. Meyer, Phys. Rev. B 65 (2002) 075207.
[65] Z. Yang, Y. Li, D.C. Look, H.M. Zhou, W.V. Chen, R.K. Kawakami, P.K.L. Yu, J.L. Liu, Thermal annealing effect on spin coherence in ZnO single crystals (unpublished).
[66] S. Ghosh, V. Sih, W.H. Lau, D.D. Awschalom, S.-Y. Bae, S. Wang, S. Vaidya, G. Chapline, Appl. Phys. Lett. 86 (2005) 232507.
[67] S. Ghosh, D.W. Steuerman, B. Maertz, K. Ohtani, H. Xu, H. Ohno, D.D. Awschalom, Appl. Phys. Lett. 92 (2008) 162109.
[68] N. Janβen, K.M. Whitaker, D.R. Gamelin, R. Bratschitsch, Nano Lett. 8 (2008) 1991.
[69] W. Pacuski, D. Ferrand, J. Cibert, C. Deparis, J.A. Gaj, P. Kossacki, C. Morhain, Phys. Rev. B 73 (2006) 035214.
[70] E. Przeździecka, E. Kamińska, M. Kiecana, M. Sawicki, Ł. Kłopotowski, W. Pacuski, J. Kossut, Solid State Commun. 139 (2006) 541.
[71] T. Dietl, Phys. Rev. B 77 (2008) 085208.
[72] R.C. O'Handley, Modern Magnetic Materials, John Wiley & Sons, 2000.
[73] I.A. Campbell, A. Fert, Transport properties of ferromagnets, in: E.P. Wohlfarth (Ed.), Ferromagnetic Materials, vol. 3, North Holland Publishing Company, 1982 (Chapter 9).
[74] N. Nagaosa, J. Sinova, S. Onoda, A.H. MacDonald, N.P. Ong, Rev. Mod. Phys. 82 (2010) 1539.
[75] J. Cumings, L.S. Moore, H.T. Chou, K.C. Ku, G. Xiang, S.A. Crooker, N. Samarth, D. Goldhaber-Gordon, Phys. Rev. Lett. 96 (2006) 196404.
[76] T. Andrearczyk, J. Jaroszyński, G. Grabecki, T. Dietl, T. Fukumura, M. Kawasaki, Phys. Rev. B 72 (2005) 121309(R).